Geochemical Perspectives Letters

Redox transfer at subduction zones: insights from Fe isotopes in the Mariana forearc

B. Debret, C.D.J. Reekie, N. Mattielli, H. Beunon, B. Ménez, I.P. Savov, H.M. Williams

Supplementary Information

The Supplementary Information includes:

- Method
- Tables S-1 and S-2
- Figures S-1 to S-4
- Supplementary Information References

Method

Major and trace elements compositions of the ultramafic clasts are from Debret *et al.*, 2019. FeO analyses of bulk-rock (BR) samples were performed at the SARM-CRPG (Nancy, France). These analyses were done by automatic titration at the equivalent point with potassium dichromate after dissolution of the sample in a HF/H_2SO_4 mixture, in the presence of H_3BO_3 and H_3PO_4. Subsequently, $Fe^{3+}/\Sigma Fe$ ratios were calculated from the measured $Fe_2O_3^{Tot}$ (BR) and FeO^{Tot} (BR) values. The error on the FeO analyses is lower than 0.05 wt. % (2sd) based on repeated analyses of UB-N serpentinite standard (CRPG-standard). The method has been tested by Debret *et al.* (2015), who were able to match measured bulk $Fe^{3+}/\Sigma Fe$ ratios with those recalculated from µ-XANES measurements of serpentine minerals (see Debret *et al.*, 2014, 2015 for method details, including standards, precision and calibration data for XANES measurements). Reference material values UB-N (FeO = 2.86 wt. %) and BIR (FeO = 8.59 wt. %) are in agreement with previous studies (e.g., Amonette and Scott, 1991; $FeO_{(UB\text{-}N)}$ = 3.01 wt. %; $FeO_{(BIR)}$ = 8.53 wt. %).

For Fe isotope measurements, ~50 mg of powdered samples were dissolved using a 1:1 mix of concentrated HF and HCl in Parr bombs at 160 °C in an oven for 5 days. These were then further dissolved with aqua regia, a 1:3 mix of concentrated HNO_3 and HCl, for 3 days at 130 °C. Finally, samples were brought into solution in 6 M HCl prior to column chemistry. This intensive procedure ensures full dissolution of refractory phases such as spinel. Quantitative purifications of Fe were achieved by chromatographic exchange, using 1 ml of AG1-x8 (200–400 mesh) and 0.4 × 7 cm Teflon columns, following the procedure developed by Sossi *et al.* (2015). All reagents used in the chemistry and mass spectrometry procedures were distilled and subboiled using Teflon two-bottle stills. The total procedural blank contribution was < 80 ng of Fe, which is negligible compared to the amount of Fe loaded on the columns (blank contribution is << 1%). Iron isotopes analyses were obtained at the University of Cambridge (UK) on a Thermo Neptune Plus multiple-collector inductively coupled plasma mass spectrometer (MC-ICP-MS). The analyses were performed in wet plasma mode. Instrumental mass fractionation was corrected by sample-standard bracketing to the IRMM-014 Fe standard.

During MC-ICP-MS measurements, analysed solutions consisted of 2 ppm natural Fe in 0.1M HNO3. The Fe beam intensities in medium resolution mode typically varied between 25 and 35V ^{56}Fe for a standard $10^{11}\Omega$ resistor. Isotope ratios are reported as $\delta^{56}Fe$ in permil notation relative to IRMM-014 external standard, and $\delta^{57}Fe$ is given to demonstrate mass dependency of the measurements. All reported errors are 2 standard deviations (2sd).

$$\delta^{56}Fe = ((^{56}Fe/^{54}Fe_{sample}) / (^{56}Fe/^{54}Fe_{IRMM\text{-}014}) - 1) \times 10^3$$

$$\delta^{57}Fe = ((^{57}Fe/^{54}Fe_{sample}) / (^{57}Fe/^{54}Fe_{IRMM\text{-}014}) - 1) \times 10^3$$

Mass dependence, long-term reproducibility and accuracy were evaluated by repeated analysis of an in-house FeCl salt standard ($\delta^{56}Fe$ = -0.73 ± 0.03 ‰; $\delta^{57}Fe$ = -1.08 ± 0.06 ‰ 2sd, n = 50) previously analysed in other studies (Millet *et al.*, 2012; Weyer and Ionov, 2007; Williams and Bizimis, 2014). In addition, reference materials (UB-N serpentinites, JP-1, DTS-2b and PCC1 peridotites) were processed through columns and analysed for Fe stable isotopes alongside samples. The data for these are displayed in Table S-1 and are in good agreement with previous studies.

Supplementary Tables

Table S-1 Critical parameters of the Mariana mud volcanoes (after Fryer *et al.*, 2018). Depth-to-slab was determined by seismic reflection profile for Yinazao, Fantangisña and Asùt Tesoro (Oakley *et al.*, 2007, 2008; Oakley, 2008), and by equilibrium mineral assemblages in metamafic clasts for South Chamorro (Maekawa *et al.*, 1993; Fryer *et al.*, 2006). Distance to trench and temperature of slab from Hulme *et al.* (2010). Depth-to-slab measurements for Yinazao, Fantangisna, and Asùt Tesoro from Oakley *et al.* (2008) and Oakley (2008). Depth-to-slab measurements for South Chamorro are extrapolation estimates (see Fryer *et al.*, 2018).

	Yinazao	Fantangisña	Asùt Tesoru	S. Chamorro
Distance to trench (km)	55	62	72	78
Depth to slab (km)	13	14	18	19
Temperature of slab (°C)	~80°	~150°	~250°	~300°

Table S-2 Iron redox state ($Fe^{3+}/\Sigma Fe$) and isotope analyses ($\delta^{56}Fe$ and $\delta^{57}Fe$, in ‰) of the studied samples. The trace element data are from Debret *et al.* (2019), B and Zn concentrations are reported in ppm.

Seamount	Label identifier	$Fe^{3+}/\Sigma Fe$	$\delta^{56}Fe$	2sd	$\delta^{57}Fe$	2sd	n	Al_2O_3/SiO_2	B	Zn	As/Yb	Sr/Yb
IODP expedition 366												
Blue Serpentinites:												
Yinazao	U1492C-5F-2-W 25/28	0.33	0.05	0.03	0.08	0.03	6	0.007	7	73		
Yinazao	U1492C-5F-3-W 43/47	0.66	-0.07	0.05	-0.10	0.09	3	0.022	6.7	73	40	914
Yinazao	U1492A-1H-2-W 139/140	0.77	0.00	0.02	0.03	0.13	3	0.020	240	66	45	212
Yinazao	U1492A-1H-3-(115-135)	0.69	0.05	0.01	0.08	0.04	3	0.024	165	61	30	281
Yinazao	U1492C-12F-2-W 19/22	0.56	-0.01	0.02	-0.01	0.02	6	0.020	7.9	58	37	986
Fantangisña	U1497A-3G-CC-W 9/10	0.62	-0.01	0.05	-0.03	0.03	3	0.015	93	76	139	262
Fantangisña	U1498B-3R-3-W 89/92	0.58	-	-	-	-	-	0.016	18.7	100	83	611
Fantangisña	U1498B-13R-1-W 37/45	0.46	-0.04	0.02	-0.05	0.03	6	0.024	26.7	56	97	500
Asùt Tesoru	U1496B-5F-1-W 77/82	0.56	-0.02	0.04	-0.05	0.07	3	0.017	10.7	96	84	778
Liz-Serpentinites:												
Asùt Tesoru	U1493B-9X-1-W 56/58	0.24	-0.12	0.03	-0.17	0.03	4	0.008	20.7	48	309	248
Asùt Tesoru	U1493B-9X-CC-W 4/9	0.37	0.09	0.02	0.13	0.03	3	0.020	29.7	65	43	556
Asùt Tesoru	U1493B-9X-CC-W 14/16	0.37	-0.03	0.03	-0.05	0.04	6	0.013	29.5	56	89	775
Atg/Liz-Serpentinites:												
Asùt Tesoru	U1495B-3G-CC-W 5/7	0.59	-0.21	0.05	-0.31	0.03	6	0.011	58.5	49	447	344
Asùt Tesoru	U1495B-3G-CC-W 24/26	0.33	0.00	0.02	0.01	0.04	6	0.003	47.7	48	377	725
Fantangisña	U1497A-13G-CC-W 52/55	0.57	-0.04	0.02	-0.06	0.03	6	0.013	48	55	160	149
Atg-Serpentinites:												
Asùt Tesoru	U1495B-5G-CC-W 17/20	0.57	-0.05	0.05	-0.07	0.05	6	0.016	16	52	101	67
Asùt Tesoru	U1495B-6F-CC-W 10/12	0.54	0.00	0.03	0.01	0.03	6	0.014	9.8	36	512	121
Asùt Tesoru	U1495A-3G-CC-W 13/15	0.51	-0.09	0.01	-0.14	0.02	6	0.021	39.4	44	360	12
Asùt Tesoru	U1495A-4F-1-W 86/89	0.52	-0.08	0.02	-0.12	0.04	6	0.023	48.6	52	232	8
Fantangisña	U1497B-4G-1-W 3/5	0.67	-0.14	0.00	-0.20	0.01	3	0.003	95	33	1783	185
Fantangisña	U1497B-4G-1-W 8/12	0.65	-0.23	0.01	-0.35	0.01	3	0.003	94.7	32	865	85
Fantangisña	U1497B-4G-1-W 3/6	0.65	-0.26	0.06	-0.47	0.07	3	0.003	96.7	33	2696	277

ODP Leg 195 expedition												
South Chamorro	1200A-7R-02-3/5	-	-0.12	0.06	-0.19	0.05	3	-	-	-	-	-
South Chamorro	1200A-11R-01-69/72	-	0.00	0.01	0.01	0.04	3	-	-	-	-	-
South Chamorro	1200A-12R-01-3/5	-	-0.20	0.01	-0.27	0.04	3	-	-	-	-	-
South Chamorro	1200A-15R-01-11/13	-	-0.11	0.03	-0.16	0.07	3	-	-	-	-	-
South Chamorro	1200A-3R-01-81/84	-	0.01	0.01	0.02	0.04	3	-	-	-	-	-
South Chamorro	1200A-13R-02-12/15	-	0.00	0.01	0.01	0.02	3	-	-	-	-	-
South Chamorro	1200A-7R-01-4/6	-	0.01	0.03	0.01	0.06	3	-	-	-	-	-
South Chamorro	1200A-16R-02-48/50	-	-0.02	0.00	0.00	0.00	3	-	-	-	-	-
Standards												
	PCC-1 (peridotite)	-	0.01	0.02	0.02	0.04	4	-	-	-	-	-
	replicate	-	0.01	0.04	0.03	0.05	3	-	-	-	-	-
	JP-1 (dunite)	-	-0.01	0.03	0.01	0.06	3	-	-	-	-	-
	replicate	-	-0.01	0.02	0.00	0.03	3	-	-	-	-	-
	DTS-2b (dunite)	-	0.00	0.02	0.00	0.05	3	-	-	-	-	-
	UB-N (serpentinite)	-	0.04	0.02	0.07	0.03	3	-	-	-	-	-
	replicate	-	0.03	0.01	0.06	0.03	3	-	-	-	-	-

Supplementary Figures

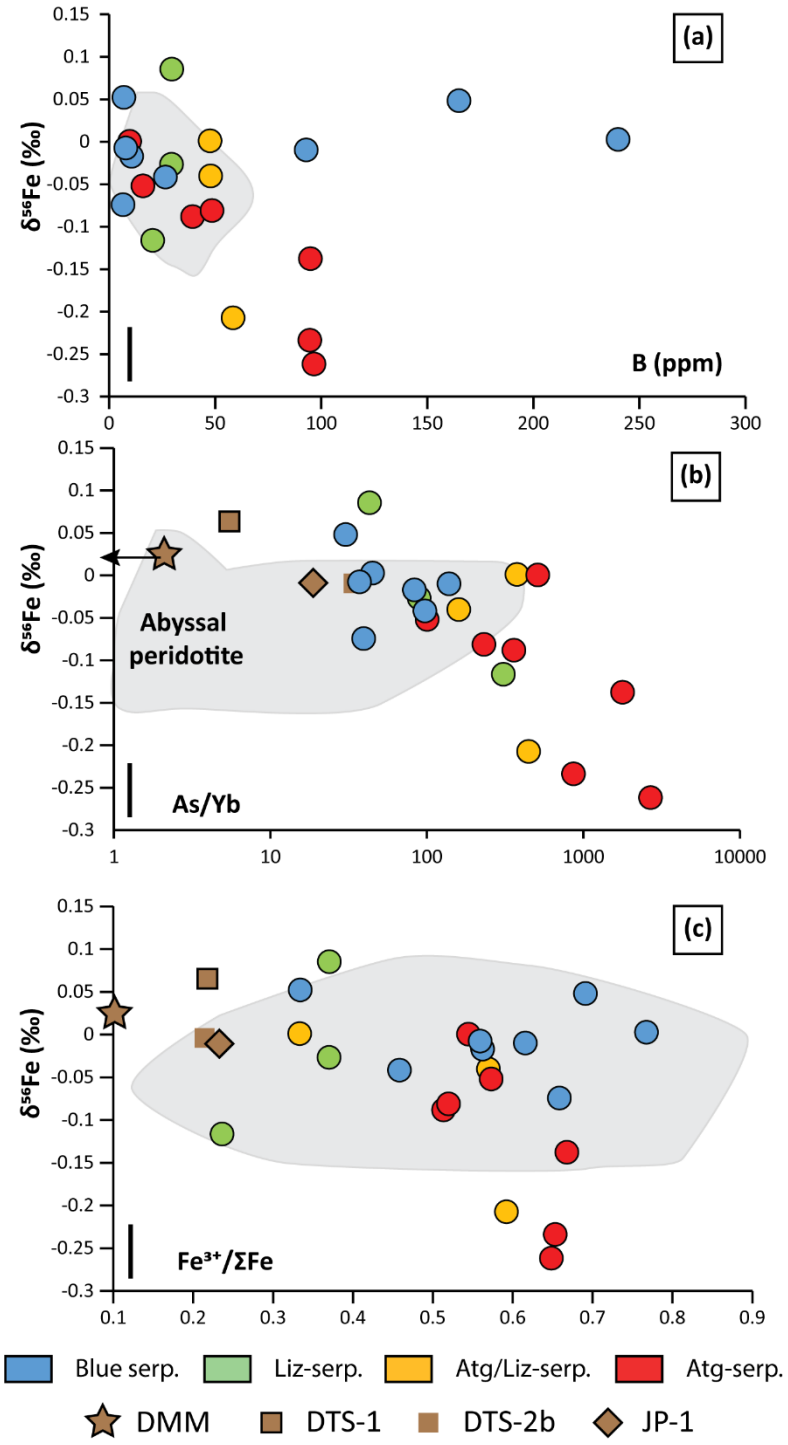

Figure S-1 Plots of $\delta^{56}Fe$ versus slab derived fluids proxies (**a-b**) and $Fe^{3+}/\Sigma Fe$ (**c**). Note that no correlation between blue-serpentinites and slab derived fluids or redox proxies have been observed showing that low pressure serpentinization stages are unable to fractionate Fe isotopes. This is in good agreement with abyssal peridotites analyses which are close to primitive mantle values. The abyssal peridotite field is from Debret *et al.* (2018). The black bars represent the standard reproducibility.

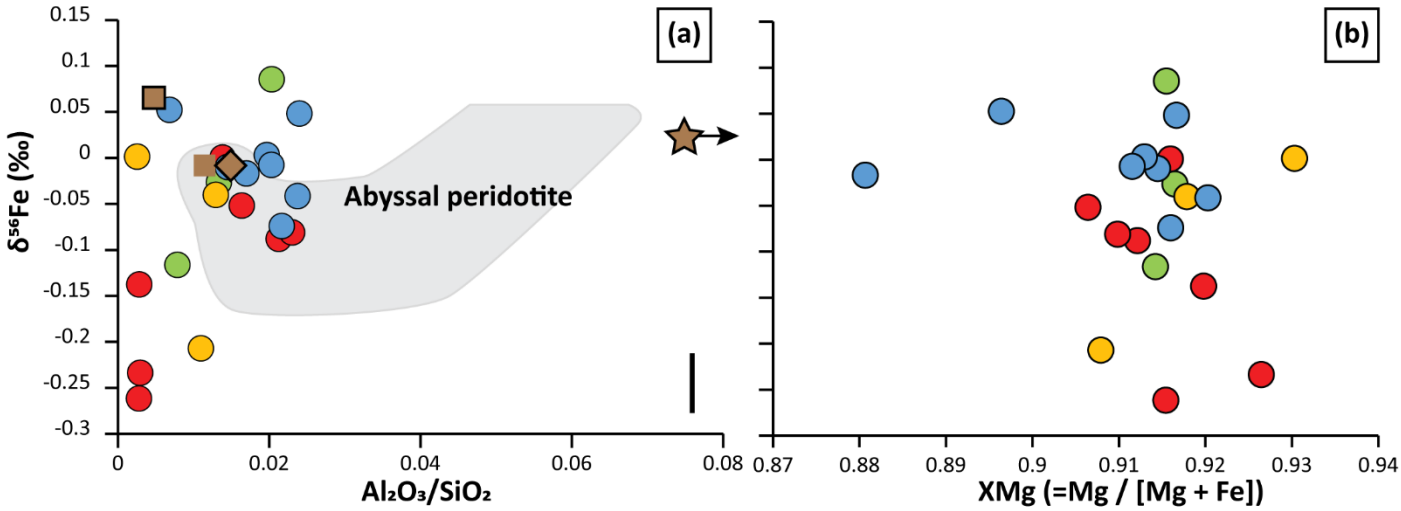

Figure S-2 Plots of δ^{56}Fe versus rock fertility (**a**) and high temperature metasomatic (**b**) proxies. No correlation between δ^{56}Fe and neither rock fertility and high temperature metasomatic proxies have been observed.

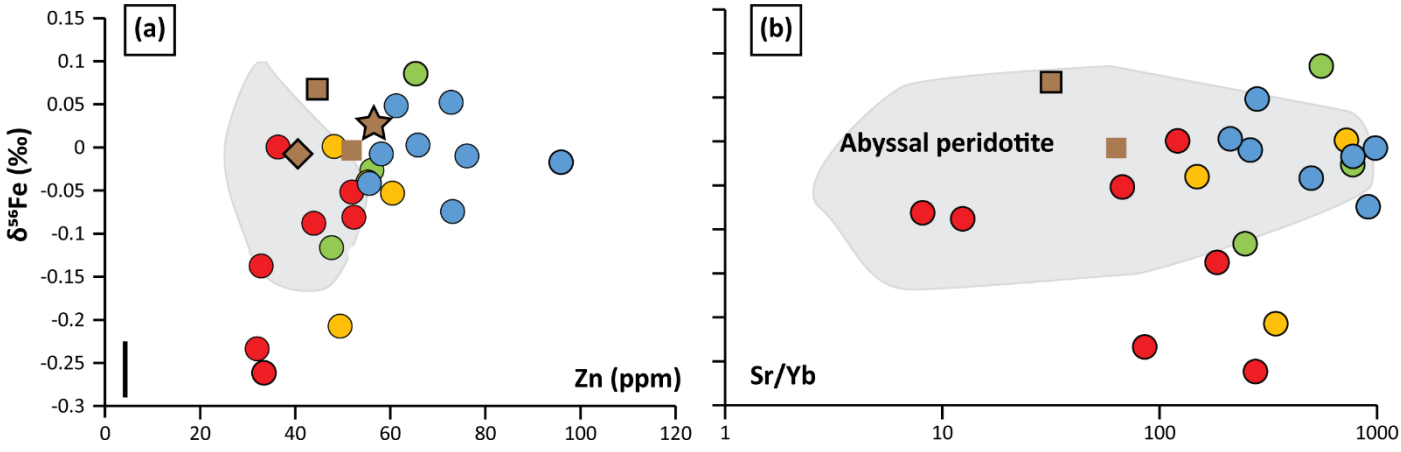

Figure S-3 Plots of δ^{56}Fe versus late stages of serpentinization (**a**) or carbonation (**b**) proxies.

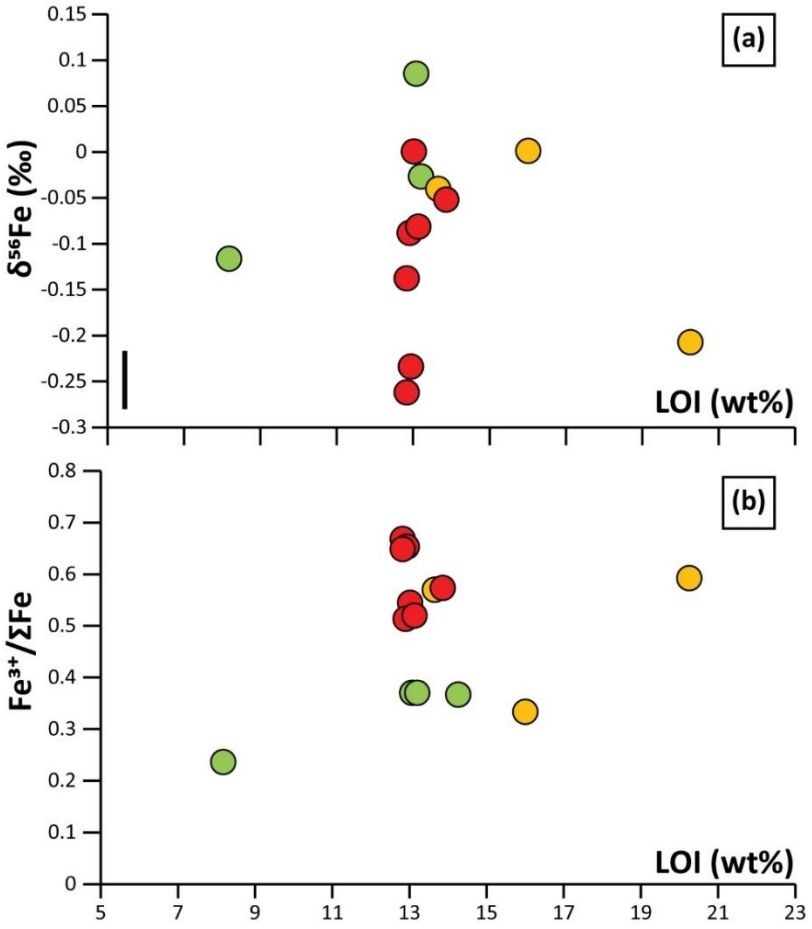

Figure S-4 Plots of δ^{56}Fe (**a**) and $Fe^{3+}/\Sigma Fe$ (**b**) versus serpentinization degree proxy (Loss On Ignition, LOI).

Supplementary Information References

Debret, B., Andreani, M., Muñoz, M., Bolfan-Casanova, N., Carlut, J., Nicollet, C., Schwartz, S., Trcera, N. (2014) Evolution of Fe redox state in serpentine during subduction. *Earth and Planetary Science Letters* 400.

Debret, B., Bolfan-Casanova, N., Padron-Navarta, J.A., Martin-Hernandez, F., Andreani, M., Garrido, C., López Sánchez-Vizcaíno, V., Gómez-Pugnaire, M.T., Muñoz, M., Trcera, N. (2015) Redox state of iron during high-pressure serpentinite dehydration. *Contributions to Mineralogy and Petrology* 169.

Debret, B., Beunon, H., Mattielli, N., Andreani, M., Ribeiro da Costa, I., Escartin, J. (2018a) Ore component mobility, transport and mineralization at mid-oceanic ridges: A stable isotopes (Zn, Cu and Fe) study of the Rainbow massif (Mid-Atlantic Ridge 36°14′N). *Earth and Planetary Science Letters* 503, 170-180.

Debret, B., Bouilhol, P., Pons, M.L., Williams, H. (2018b) Carbonate Transfer during the Onset of Slab Devolatilization: New Insights from Fe and Zn Stable Isotopes. *Journal of Petrology* 59, 1145–1166.

Debret, B., Albers, E., Walter, B., Price, R., Barnes, J. D., Beunon, H., Facq, S., Gillikin, D.P., Mattielli, N., Williams, H., (2019) Shallow forearc mantle dynamics and geochemistry: New insights from the IODP expedition 366. *Lithos* 326–327, 230–245.

Fryer, P., Gharib, J., Ross, K., Savov, I., Mottl, M.J. (2006) Variability in serpentinite mudflow mechanisms and sources: ODP drilling results on Mariana forearc seamounts. *Geochemistry, Geophysics, Geosystems* 7, Q08014.

Fryer, P., Wheat, C.G., Williams, T., Scientists Expedition, 366 (2018) Mariana Convergent Margin and South Chamorro Seamount. *Proceedings of the International Ocean Discovery Program* 366.

Maekawa, H., Shozui, M., Ishii, T., Fryer, P., Pearce, J.A. (1993) Blueschist metamorphism in an active subduction zone. *Nature* 364, 520–523.

Millet, M.A., Baker, J.A., Payne, C.E. (2012) Ultra-precise stable Fe isotope measurements by high resolution multiple-collector inductively coupled plasma mass spectrometry with a 57Fe- 58Fe double spike. *Chemical Geology* 304–305, 18–25.

Oakley, A. (2008) A multi-channel seismic and bathymeric investigation of the central Mariana convergent margin [Ph.D. dissertation]. University of Hawaii. http://www.soest.hawaii.edu/GG/resources/theses/Oakley Dissertation 2008.pdf

Oakley, A.J., Taylor, B., Fryer, P., Moore, G.F., Goodliffe, A.M., Morgan, J.K. (2007) Emplacement, growth, and gravitational deformation of serpentinite seamounts on the Mariana forearc. *Geophysical Journal International* 170, 615–634.

Oakley, A.J., Taylor, B., Moore, G.F. (2008) Pacific plate subduction beneath the central Mariana and Izu-Bonin fore arcs: new insights from an old margin. *Geochemistry, Geophysics, Geosystems* 9, Q06003.

Sossi, P.A., Halverson, G.P., Nebel, O., Eggins, S.M. (2015) Combined separation of Cu, Fe and Zn from rock matrices and improved analytical protocols for stable isotope determination. *Geostandards and Geoanalytical Research* 39, 129–149.

Weyer, S., Ionov, D.A. (2007) Partial melting and melt percolation in the mantle: The message from Fe isotopes. *Earth and Planetary Science Letters* 259, 119–133.

Williams, H.M., Bizimis, M. (2014) Iron isotope tracing of mantle heterogeneity within the source regions of oceanic basalts. *Earth and Planetary Science Letters* 404, 396–407.